Vagal Nerve Stimulation Triggers Wide-Spread Evoked Responses and Changes in Large-Scale Functional Connectivity in Rat Brains

Jiayue Cao[1,4], Kun-Han Lu[2,4], Terry Powley[1,3,4], and Zhongming Liu[1,2,4*]

[1]*Weldon School of Biomedical Engineering,*

[2]*School of Electrical and Computer Engineering,*

[3]*Department of Psychological Science,*

[4]*Purdue Institute of Integrative Neuroscience*

Purdue University, West Lafayette, Indiana, United States

***Correspondence**

Zhongming Liu, PhD

Assistant Professor of Biomedical Engineering

Assistant Professor of Electrical and Computer Engineering

College of Engineering, Purdue University

206 S. Martin Jischke Dr.

West Lafayette, IN 47907, USA

Phone: +1 765 496 1872

Fax: +1 765 496 1459

Email: zmliu@purdue.edu

Abstract

Background: Vagus nerve stimulation (VNS) is a FDA-approved therapy for epilepsy and depression. However, the efficacy of VNS varies, and its mechanism is unclear. Prior studies have used functional magnetic resonance imaging (fMRI) to map brain activations with VNS in human brains but yielded inconsistent findings. The source of the inconsistency might be attributed to the complex temporal characteristics of VNS-evoked responses that cannot be fully explained by simplified response models.

Objective: We used fMRI to characterize the effects of VNS in rat brains without assuming any *priori* response model. The questions of primary interest were 1) whether and where the VNS evoked responses at the level of networks, and 2) whether and where the VNS altered the patterns of interactions among intrinsic functional networks.

Methods: We performed 7-Tesla blood oxygenation level dependent (BOLD) fMRI on Sprague–Dawley rats receiving simultaneous electrical stimulation at the left cervical vagus nerve. Using independent component analysis, we mapped the patterns of network activations and interactions in contrast to those in the resting state.

Results: Left cervical VNS evoked widespread responses over ~76% of the brain volume with the most notable activations in the brainstem and hypothalamus. The VNS evoked complex and distinctive temporal responses at different brain networks and altered the patterns of interactions among networks, especially for the limbic system.

Conclusion: This paper reports a method for exploring the complex response of VNS in a data-driven manner. The results suggest that VNS evokes wide-spread BOLD responses and alters large-scale functional connectivity.

Keywords: vagal nerve stimulation, functional magnetic resonance imaging, model-free analysis**,** brain-wide response

Abbreviations: blood oxygenation level dependent (BOLD), central neural system (CNS), functional magnetic resonance imaging (fMRI), general linear model (GLM), hemodynamic response function (HRF), independent components (ICs), independent component analysis (ICA), vagus nerve stimulation (VNS)

Acknowledgements: Thank Dr. Nanyin Zhang for sharing the functional atlas of the rat brain. Thank Elizabeth Baronowsky and Dr. Matthew Ward for their assistance in the initial training in animal surgery.

Funding: This work was supported by the National Institutes of Health [grant numbers, 1OT2TR001965-01, R01MH104402].

Introduction

Since the 1800s (1, 2), vagus nerve stimulation (VNS) has been studied as a potential way to treat various diseases, including epilepsy, depression, tinnitus, Alzheimer's Disease, and obesity (3-8). The therapeutic benefits apparently depend on the effects of VNS on the central neural system (CNS) mediated through neuroelectrical or neurochemical signaling (9). Studies have been conducted to evaluate the CNS responses to VNS with various techniques. For example, invasive recordings of unit activity or field potentials have shown VNS-evoked neuronal responses in the nucleus of solitary tract (10), the locus coeruleus (11), and the hippocampus (12). These techniques offer high neuronal specificity but only cover spatially confined targets. In contrast, electroencephalogram (EEG) has been used to reveal VNS-induced synchronization or desynchronization of neural oscillations in the macroscopic scale (13, 14), while being severely limited by its spatial resolution and specificity as well as its inability to detect activity from deep brain structures. However, sub-cortical regions are of interest for VNS, because the vagus nerves convey signals to the brain through polysynaptic neural pathways by projecting to the brainstem, then subcortical areas, and lastly the cortex (9, 15).

Complementary to conventional electrophysiological approaches, functional neuroimaging allows characterizing the effects of VNS throughout the brain volume. Using positron emission tomography (PET) or single-photon emission computerized tomography (SPECT), prior studies have reported VNS evoked responses in the thalamus, hippocampus, amygdala, inferior cerebellum, and cingulate cortex (16-19); but these techniques are unable to capture the dynamics of responses due to their poor temporal resolution. In this regard, functional magnetic resonance imaging (fMRI) is more favorable because it offers balanced and higher spatial and temporal resolution. Previous human VNS-fMRI studies have reported VNS-evoked blood oxygenation level dependent (BOLD) responses in the thalamus, hypothalamus, prefrontal cortex, amygdala, and hippocampal formation (20-24). However, the reported activation patterns vary notably across existing studies (25), highlighting different regions responding to the VNS or the same regions with the opposite responses (20, 22). The variation may implicate the diversity of VNS' therapeutic effects in

83 different clinical subjcts but could also be attributable to the different analysis protocols (25). Therefore,
84 before moving forward and evaluating VNS' therapeutic effects using fMRI, it is necessary to verify
85 reliability of the current analysis method or develop a more reliable method for analyzing VNS-evoked
86 BOLD responses.

87 Functional MRI not only localizes the CNS responses of VNS (25), it also reveals the patterns and
88 dynamics of functional networks during VNS. Characterizing the network-level effect of VNS has been
89 central to understanding the mechanisms of VNS-based therapetutics. For example, given a lesion in the
90 locus coruleus, VNS fails to suppress epilepsy (26). Given blockade of the muscarinic receptor, VNS fails
91 to promote perceptual learning (27). These findings support the notion that VNS alters large-scale
92 functional networks in part through the adrenergic and cholinergic systems. However, how VNS affects the
93 patterns of temporal interactions among regions or networks (or functional connectivity) has rarely been
94 addressed (28), while fMRI has become the primary tool for studying functional connectivity in the resting
95 state (29, 30).

96 In this study, we aimed to address the BOLD effects of VNS in rat brains. Compared to human
97 studies, the use of animal models allowed us to minimize the inter-subject variation in genetics, gender,
98 age, weight, and health conditions. In such well-controlled conditions, the effects of VNS were mapped and
99 characterized in the whole brain by using BOLD-fMRI at 7-T. Our first goal was to verify the analysis
100 method as one of the sources of variation in VNS-fMRI studies and to apply a data-driven activation
101 mapping method, namely independent component analysis (ICA), to avoid the potential limitations or bias.
102 When studying the VNS effects, the primary effects of interest include not only the locations and dynamics
103 of VNS-evoked activations but also the changes in large-scale functional connectivity during VNS relative
104 to the resting state .

105

Methods and Materials

Subjects

A total of 17 Sprague–Dawley rats (male, weight: 250-350g; Envigo RMS, Indianapolis, IN) were studied according to a protocol approved by the Purdue Animal Care and Use Committee (PACUC) and the Laboratory Animal Program (LAP). Of the 17 animals, seven animals were used for VNS-fMRI experiments; ten animals were used for resting state fMRI. All animals were housed in a strictly controlled environment (temperature 21±1°C and 12 h light-dark cycle, lights on at 6:00 AM, lights off at 6:00 PM).

Animal preparation

For the VNS-fMRI experiments, each animal was initially anesthetized with 5% isoflurane and maintained with continuous administration of 2-3% isoflurane mixed with oxygen and a bolus of Rimadyl (5 mg/Kg, Zoetis) administrated subcutaneously. After a toe-pinch check for adequate anesthesia, a 2-3cm midline incision was made starting at the jawline and moving caudally. The left cervical vagus nerve was exposed and isolated by removing the surrounding tissue. A bipolar cuff electrode (Microprobes, made of platinum, with 1mm distance between contacts) was then wrapped around the exposed vagus nerve. For resting-state fMRI experiments, animals were anesthetized with the same dose of isoflurane without the aforementioned surgical procedures.

Once animals were moved to the MRI scanner, their heads were constrained with customized head restrainer. Then a bolus of dexdomitor (7.5 µg/Kg, Zoetis) was administrated subcutaneously. At about 15-20 mins following the bolus injection, dexdomitor was subcutaneously infused at 15 µg/Kg/h and increase every hour as needed (31). Isoflurane was reduced to be 0.1-0.5% mixed with oxygen. Both the dexdomitor infusion rate and the isoflurane dose were adjusted to maintain the respiration between 40 to 70 times per min and the heart rate between 250 to 350 beats per minute.

Vagus nerve stimulation

The bipolar cuff electrode was connected to a current stimulator (model 2200, A-M system) placed outside of the MRI room through a 3-m twisted-pair of copper wire. Stimulation current was delivered in 10s-ON-50s-OFF cycles. When it was ON, biphasic square pulses (pulse width: 0.1 ms; amplitude: 1.0 mA; frequency: 10 Hz) were delivered. For a total of 10 mins, ten cycles of stimulation were delivered in each imaging session. Resting (stimulation-free) at least one minute long was given between sessions. Up to 4 sessions were scanned for each animal. Fig. 1 illustrates the VNS paradigm.

MRI and fMRI

MRI data were acquired with a 7-T small-animal MRI system (BioSpec 70/30, Bruker) equipped with a volume transmitter coil (86 mm inner diameter) and 4-channel surface receiver coil. After localizer scans, T2-weighted anatomical images were acquired with a rapid acquisition with relaxation enhancement (RARE) sequence (repetition time (TR)=5804.607s, effective echo time (TE)=32.5ms, echo spacing=10.83 ms, voxel size=$0.125\times0.125\times0.5\text{mm}^3$, RARE factor=8, flip angle (FA)=90°). The BOLD fMRI data were acquired by using a 2-D single-shot gradient echo echo-planar imaging (EPI) sequence (TR=1 s, TE=15 ms, FA=55°, in-plane resolution about $0.6\times0.6\ \text{mm}^2$, slice thickness=1 mm). In the VNS group, the VNS was delivered with the aforementioned block-design paradigm during continuous EPI.

Throughout the imaging experiment, the animal's body temperature was maintained at 37 ± 0.5 °C using an animal-heating system. The oxygen saturation level (SpO_2) was maintained above 96%. Heart rate and respiration rate were monitored with a small-animal physiological monitoring system (Kent Scientific).

Data preprocessing

MRI and fMRI data were preprocessed by using Analysis of Functional Neuroimages (AFNI) and custom-built functions in MATLAB. Within each session, the fMRI data were corrected for motion, by registering every volume to the first volume using *3dvolreg*. After removing the first ten volumes, *retroicor* was used to correct for the motion artifacts due to respiratory and cardiac activity (32, 33). Then, *slicetimer*

152 was used to correct the timing for each slice. For each animal, we first normalized the EPI image to its T_2
153 weighted structural images and then registered to the template (34) using *flirt*. Motion artifact was further
154 removed by regressing out the six motion-correction parameters. The fMRI data were then spatially
155 smoothed with a 3-D Gaussian kernel with 0.5-mm full width at half maximum (FWHM). The fMRI time
156 series were detrended by regressing out a 2rd-order polynomial function voxel by voxel.

157 ***General linear model analysis***

158 We explored using the conventional general linear model (GLM) analysis to map the activations
159 evoked by VNS as in previous studies (23, 24, 35-37). Specifically, we derived a response model by
160 convolving the stimulation block (modeled as a box-car function) with a canonical hemodynamic response
161 function (HRF) (modeled as a gamma function). For each session, the fMRI signal at every voxel was
162 correlated with this response model. The correlation coefficient was converted to a z-score by using the
163 Fisher's z-transform. The voxel-wise z-score was averaged across sessions and evaluated for statistical
164 significance with one-sample t-test ($p<0.05$, uncorrected).

165 This analysis revealed the group-level brain activation with VNS given an assumed response model.
166 Since the validity of this response model for VNS was not established, we intentionally varied the response
167 model by assuming three different peak delays (3s, 6s, or 9s) in the HRF. We compared the activation maps
168 obtained with the three different response models, to assess the dependence of the resulting activation map
169 on the presumed response characteristics.

170 ***Independent component analysis***

171 In contrast to the voxel-wise general linear model (GLM) analysis, we used ICA to map networks
172 and their responses to VNS in a data-driven or model-free manner. For each session and each voxel, the
173 fMRI signal during VNS was demeaned and divided by its standard deviation. The resulting fMRI data
174 were then concatenated across all VNS-fMRI sessions. Infomax ICA (38) was used to decompose the
175 concatenated data into 20 spatially independent components (ICs). Each of these ICs included a spatial map

176 and a time series, representing a brain network and its temporal dynamics, respectively. In the spatial maps
177 of individual ICs, the intensities at each given voxel represented the weights by which the time series of
178 corresponding ICs were combined to explain this voxel's fMRI time series. Such weights were converted
179 to Z-statistics and then thresholded as described in a previous paper (39). The threshold was selected such
180 that the false negative rate was three times as large as the false positive rate. To obtain the false negative
181 and positive rates, the Z-statistics of all voxels in an IC map were modeled as a two-Gaussian mixture
182 distributions: one representing the noise, the other representing the signal.

183 Following ICA, we evaluated the VNS-evoked response separately for each IC, instead of each
184 voxel. To do so, each IC's time series was segmented for every VNS block. Each segment lasted 54 seconds,
185 starting from 3 seconds before the onset of a VNS block to 41 seconds after the offset of this block, while
186 the block size was 10 seconds. To address whether an IC responded to the VNS, we treated each time point
187 as a random variable and each segment as an independent sample. One-way analysis of variance (ANOVA)
188 test was conducted against a null hypothesis that there was no difference among all the time points (meaning
189 no response). The ICs that were statistically significant (p<5e-6) were considered as activated by VNS.

190 For each activated IC, we further characterized its temporal response to VNS. Briefly, we identified
191 the time points during or after the VNS block, where the signals significantly differed from the pre-stimulus
192 baseline by using Tukey's honest significant difference (HSD) test as post-hoc analysis following the
193 previous ANOVA test. Following this statistical test, the VNS-activated ICs were further classified into
194 three types (i.e. positive, negative, and mixed) of responses by visual inspection.

195 ***Functional connectivity analysis***

196 We further addressed whether VNS altered the patterns of temporal interactions among functional
197 networks identified by ICA. To do so, the voxel time series was demeaned and standardized for each fMRI
198 session including both VNS and resting conditions. The fMRI data were concatenated across all sessions
199 and were then decomposed by ICA to yield 20 spatially ICs or networks, along with their corresponding

time series. The first IC was removed because it was identified as the global component. The time series of the rest ICs were divided into the signals corresponding to the VNS sessions, and those corresponding to all resting-state sessions.

We defined the functional connectivity between networks as the temporal correlations between the ICs. The correlations were evaluated separately for the resting and VNS conditions and all pairs of ICs. Based on their temporal correlations, we grouped the ICs into clusters by applying k-means clustering method (with squared Euclidean distance) to ICs' temporal correlation matrix. As a result, the correlations tended to be stronger within clusters than between clusters.

We further evaluated the differences in functional connectivity between the VNS condition and the resting state. For this purpose, the functional connectivity between ICs was evaluated for each VNS session, as well as each resting-state session. Their differences between these two conditions were evaluated using unpaired two-sample t-test ($p<0.05$, uncorrected). The functional connectivity was plotted in the functional connectogram.

Results

Model-based VNS activations were sensitive to variation of the response model

Seven rats were scanned for fMRI while their left cervical vagus nerve was electrically stimulated in a (10s-ON-50s-OFF) block-design paradigm as illustrated in Fig. 1. The BOLD response phase-locked to VNS block appeared complex and variable across regions of interest (ROIs). For example, the BOLD responses were notably different across three ROIs, namely the retrosplenial cortex (RSC), brainstem (BS), and dorsal caudate putamen (Cpu) in a functional atlas (40) of the rat brain (Fig. 2a). These responses were not readily explainable by a typical response model derived from a canonical HRF (Fig. 2b, top). The GLM analysis with three different response models (by varying the HRF peak latency with 3s increments) yielded almost entirely distinctive activation maps (Fig. 2b), each of which was only marginally significant ($p<0.05$,

224 uncorrected). Therefore, VNS-evoked BOLD responses were too complex and variable to be captured by a
225 single response model. As such, the conventional GLM analysis likely leads to incomplete and inconsistent
226 activations with VNS, which possibly accounts for the diverging findings reported in the related literature
227 (20-24).

228 ***VNS induced widespread and complex network responses***

229 We evaluated the VNS-evoked responses using a data-driven analysis method, and highlight the
230 responses at the level of networks, where the networks were identified as spatially ICs. It turned out that 15
231 out of the 20 ICs were significantly activated by VNS (one-way ANOVA, p<5e-6, Fig. 3a). Those activated
232 ICs collectively covered 76.03% of the brain volume (Fig. 3b). Among the activated regions, the brainstem
233 and the hypothalamus exhibited stronger responses than other areas.

234 The response time courses were also notably different across ICs. As shown in Fig. 3.a through 2.c.,
235 the time points, which were different from the baseline, are highlighted in red (p<0.05, Tukey's HSD). The
236 polarity of the red marked time points further characterized each IC as positive, negative, or biphasic-mixed
237 response. The negative response group included the amygdala, dorsal striatum, primary motor cortex,
238 midbrain, left somatosensory cortex, and superior cerebellum. The positive response group mainly included
239 the brainstem, thalamus, and hypothalamus region. The mixed response group included the hippocampal
240 formation, cingulate cortex, and prelimbic & infralimbic cortex. The ICs sharing similar responding polarity
241 were presumably more functionally associated with one another. Besides polarity characteristics, responses'
242 timing differences could also group ICs into long-lasting and stimulus-locked responses. Long-lasting
243 responses happened in the hippocampal formation, prefrontal cortex, amygdala. Stimulus-locked responses
244 showed in the brainstem and hypothalamus. The ICs with long-lasting responses were mostly involved in
245 high-level functions, such as forming memory, making decisions, and modulating emotion. The ICs with
246 time-locked responses had the more direct vagal projections involving fewer synapses. Considering both
247 polarity and timing differences, VNS responses varied across regions and networks and could reflect how
248 different regions changed their communications with each other. Therefore, studying the time courses

249 across different ICs could help us understand the changes of region-regions (or IC-IC) interaction altered
250 by VNS.

251 ### *VNS altered functional connectivity*

252 We evaluated the IC-IC interactions during VNS and compared with those in the resting state
253 (control group). Three clusters were obtained with k-means clustering separately for the VNS and resting-
254 state groups (Fig. 4.a). Cluster 1 was similar in both the VNS and control groups, and represented the
255 sensorimotor cortex. In contrast, cluster 2 and 3 were notably different in the two groups. For cluster 2,
256 VNS strengthened the correlations between the hippocampal formation and such regions as the retrosplenial
257 cortex relative to the resting state. For cluster 3, VNS reduced the correlations between the prefrontal cortex
258 and such regions as the basal ganglia. We further compared the functional connectivity of each IC-IC pair
259 to better illustrate the changes in temporal correlation across different regions (ICs) ($P<0.005$, *t*-test). Fig
260 4.b shows that VNS manipulated the degree of interactions among different regions in the limbic system.
261 The cingulate cortex was less correlated with the ventral striatum. The left and right hippocampal formation
262 formed stronger functional connectivity, and as a whole hippocampal formation formed stronger functional
263 connectivity with the retrosplenial cortex During VNS, the functional connectivity was not only reorganized
264 within the limbic system but also between the limbic system and the sensorimotor cortex. VNS strengthened
265 the interaction across the sensorimotor cortex with the hippocampal formation, retrosplenial cortex, and
266 dorsal striatum, but weakened the functional connectivity between the sensorimotor cortex and the cingulate
267 cortex. In summary, VNS reorganized the functional connectivity within the limbic system and altered the
268 interactions between the limbic system and the sensorimotor cortex.

269

Discussion

This paper studied VNS induced BOLD responses on seven healthy rats with the same stimulating protocol. Using data-driven analysis method, our results showed that VNS evoked brain-wide BOLD responses covering ~76% of the brain regions, but the distinct responding time courses varied across regions and were different from the canonical HRF, which was commonly used in the previous VNS-fMRI studies. In addition, VNS also altered the functional networks compared to those observed in the resting state. In particular, VNS altered functional connectivity within the limbic system and between the limbic system and the sensorimotor cortex. Such changes in functional connectivity may underlie the differential functions of VNS in modulating emotion and sensorimotor plasticity.

VNS evoke brain-wide responses

A major finding in this study was that VNS evoked time-locked and widespread BOLD responses over most parts of the brain. This finding appeared surprising at the first glance, since simulation was applied to the left cervical vagus – a seemingly narrowly-focused entry of neuromodulation. Nevertheless, previous studies suggest that neural activity may drive global fluctuations in resting-state fMRI activity (41), and simple (e.g., checkerboard) visual stimulation may evoke whole-brain fMRI responses (42). Common to those prior studies and this study may be the notion that the brain is so densely wired and interconnected that focal modulation may induce a cascade of responses through neuronal circuits. Such network responses may even have a global reach, if the stimulation innervates sub-cortical structures with distributed modulatory effects on the brain (43).

In this regard, widespread responses to VNS may be mediated through diffusive neuromodulation triggered by VNS. Vagal afferents project to the parabrachial nucleus, locus coeruleus, raphe nuclei through nucleus of solitary tract (44). From the parabrachial nucleus, locus coeruleus, and raphe nuclei, connectivity extends onto hypothalamus, thalamus, amygdala, anterior insular, infralimbic cortex, and lateral prefrontal cortex (45-48). In fact, the widespread VNS-evoked activations reported herein are consistent with the full

294 picture gathered from piecemeal activations observed in prior VNS-fMRI (see reviews in (25)),
295 transcutaneous VNS-fMRI studies (49), and EEG-fMRI studies (13, 14). In light of those results, the extent
296 of the VNS effects on the brain has been under-estimated in prior studies, likely due to the use of simplified
297 response models that fail to capture the complex and variable responses across all activated regions.

298 ***Origins and interpretation of different response characteristics***

299 Results in this study suggest that VNS induces a variety of BOLD responses that vary across regions.
300 In addition to coarse and qualitative classification of various responses as positive, negative, or mixed (first
301 negative and then positive) (Fig. 3), the responses at various regions or networks also differed in terms of
302 transient vs. sustained behaviors during and following VNS. For example, the responses at the brainstem
303 and the hypothalamus showed a very rapid rise around 2s and rapid decay around 5s following the onset of
304 VNS. Although the generalizable origins of transient BOLD responses are still debatable (50-52), we
305 interpret the transient responses to VNS as a result of direct neuroelectric signaling through the vagal nerves.
306 Nuclei in the brainstem, e.g., NTS, contain neurons receiving direct projections from the vagus, and in turn
307 connect to the hypothalamus. Such brain structures are thus well-positioned to respond rapidly to VNS.
308 Also, the rapid decay of the BOLD response in the brainstem and hypothalamus may indicate neuronal
309 adaption – a factor of consideration for designing the duration and duty cycle of VNS. However, such
310 interpretation should be taken with caution. The neurovascular coupling (modeled as the HRF) behaves as
311 a low-pass filter through which the BOLD response is generated from local neuronal responses. Although
312 the peak latency in HRF is 4 to 6s in humans, it is as short as 2s in rodents (53), making it relatively more
313 suitable for tracking transient neuronal dynamics.

314 Another intriguing observation was the prolonged BOLD responses that sustained for a long period
315 following the offset of VNS. In the striatum, hippocampus, as well as the prelimbic and infralimbic cortex,
316 the VNS-evoked response lasted for 40s or even longer, while the VNS only lasted 10s (Fig. 3). Such
317 prolonged responses suggest potentially long-lasting effects of VNS. This observation is also in line with
318 clinical studies showing that the effects of VNS on seizure suppression are not limited to the stimulation,

319 but sustain during periods in the absence of VNS (54). Moreover, those regions showing prolonged effects
320 of VNS tended to be higher-level functional areas presumably involved in learning, decision-making,
321 memory, and emotion-processing. Speculatively, it implies that the VNS-based modulation of cognitive
322 functions or dysfunctions operates in a relatively longer time scale while imposing potentially therapeutic
323 effects on a longer term.

324 ***VNS alters network-network interactions***

325 This study highlights the importance of evaluating the effects of VNS on functional connectivity,
326 which measures the degree to which regions or networks interact with each other. It is widely recognized
327 that brain functions emerge from coordination among regions (55). However, prior studies address the
328 effects of VNS in focal and target regions (56), whereas the effects of VNS on functional connectivity is
329 perhaps more functionally relevant. In line with this perspective, a recent study has shown that
330 transcutaneous VNS modulates the functional connectivity in the default mode network in patients with
331 major depressive disorders, and the change in functional connectivity is related to the therapeutic efficacy
332 across individual patients [50]. Thus, VNS may reorganize the patterns of interactions among functional
333 networks – a plausible network basis underlying VNS-based therapeutics.

334 Our results show that VNS reorganizes the functional connectivity with respect to the limbic system.
335 Relative to the intrinsic functional connectivity in the resting state, VNS increases functional connectivity
336 between the retrosplenial cortex and hippocampal formation, of which the functional roles are presumably
337 related to memory, learning, and monitoring sensory inputs (57, 58). In addition, VNS increases functional
338 connectivity between the sensory cortex and the striatum, of which the functional roles are presumably the
339 integration of sensorimotor, cognitive, and motivation/emotion (59). In contrast, VNS decreases functional
340 connectivity between the cingulate cortex and the ventral striatum, which likely affect the emotional control
341 of visceral, skeletal, and endocrine outflow (60). Collectively, these observations lead us to speculate that
342 VNS biases the limbic system to shift its functional role from emotional processing to perceptual learning.

343 Such speculation is consistent with the therapeutic effects of VNS in depression patients (61, 62) and the
344 cortical plasticity of interest to perceptual learning and motor rehabilitation induced by VNS (63, 64).

345 *Model-free activation mapping in the level of networks*

346 Central to this study is the use of model-free and data-driven analysis for mapping activations in
347 the level of networks, instead of voxels or regions. This is in contrast to conventional GLM analysis used
348 in previous VNS-fMRI studies, which assumes that neural responses sustain in the entire period of VNS,
349 and the BOLD effects of neural responses may be modeled with a canonical HRF (23, 24, 35-37). Both of
350 these assumptions may not be entirely valid. Neural responses may exhibit a range of non-linear
351 characteristics. The typical HRF model is mostly based on data or findings obtained from the cortex during
352 sensory stimulation (65), whereas no study has modeled the HRF for VNS. Moreover, the neurovascular
353 coupling may also vary across regions in the brain, especially between sub-cortical and cortical areas due
354 to their differences in local vasculatures (66). Thus, the GLM analysis with a single and empirical response
355 model most likely falls short for explaining the complex and variable responses across all brain regions.

356 The model-free analysis allowed us to detect the VNS-evoked brain response in a data-driven way
357 without assuming any prior response model. A similar strategy has been used to test for voxel-wise BOLD
358 responses to visual stimulation in humans (42). What was perhaps unique in this study was the use of the
359 model-free analysis on the activity of spatially independent components, rather than that of single voxels.
360 Each IC contained a set of voxels (or locations) that shared a common pattern of temporal dynamics. ICA
361 utilized the fact that individual voxels were organized by networks, not in isolation, to extract the network
362 activity as the time series of each IC, which reflected the (weighted) average activity of all the voxels that
363 belonged to each IC. As such, the signal-to-noise ratio was higher for IC-wise activity than for voxel-wise
364 activity, providing better sensitivity for detecting activations at the network level. This model-free analysis
365 method is thus arguably more favorable than conventional GLM analysis, especially when the response
366 characteristics are complex and unclear, e.g., given VNS.

Potentially confounding cardiac and respiratory effects

The BOLD signal is an indirect measure of neural activity. Therefore, it may be affected by non-neuronal physiological fluctuations (67). Previous studies have shown that VNS causes cardiorespiratory effects, e.g., variations in the heart rate, respiration rate, and SpO2 (68, 69). Such effects may potentially confound the interpretation of the VNS-induced BOLD responses regarding neuronal activations. Such confounding effects were highlighted in a prior study, in which VNS was found to decrease the heart rate and in turn decrease the BOLD signal throughout the rat brain (70). In this study, we were concerned about this potential confounding effect, and reduced to the pulse width of VNS to 0.1ms, instead of 0.5ms in that study (70). Such shortened pulse width largely mitigated the cardiac effects, as no obvious changes in heart rate were noticeable during experiments.

Also, the cardiac effects would manifest themselves as the common physiological response observable throughout the brain. This was not the case in this study. Despite wide-spread activations with VNS, the responses at individual regions exhibited different temporal characteristics, which could not be readily explained by a common confounding source (e.g., respiratory or cardiac). Instead, the regions with similar response patterns formed well-patterned functional networks, resembling intrinsic resting-state networks previously observed in rats (71). For these reasons, it was unlikely that the VNS-induced activation and functional-connectivity patterns were the result at non-neuronal cardiac or respiratory effects. Similar justifications are also applicable to the confounding respiratory effects. Nevertheless, future studies are desirable to fully disentangle the neuronal vs. non-neuronal effects of VNS. Of particular interest is using multi-echo fMRI to differentiate BOLD vs. non-BOLD effects (67), and combining electrophysiology and fMRI to pinpoint the neural origin of the fMRI response to VNS (72).

References

1. Gaskell WH. The Electrical changes in the Quiescent Cardiac Muscle which accompany Stimulation of the Vagus Nerve. J Physiol 1886;7(5-6):451-2.
2. Robinson C, Draper G. Studies with the electrocardiograph on the action of the vagus nerve on the human heart : II. the effects of vagus stimulation on the hearts of children with chronic valvular disease. J Exp Med 1912;15(1):14-48.
3. Ben-Menachem E. Vagus-nerve stimulation for the treatment of epilepsy. Lancet Neurol 2002;1(8):477-82.
4. George MS, Sackeim HA, Rush AJ, Marangell LB, Nahas Z, Husain MM, et al. Vagus nerve stimulation: a new tool for brain research and therapy. Biol Psychiatry 2000;47(4):287-95.
5. De Ridder D, Vanneste S, Engineer ND, Kilgard MP. Safety and efficacy of vagus nerve stimulation paired with tones for the treatment of tinnitus: a case series. Neuromodulation 2014;17(2):170-9.
6. Peña DF, Engineer ND, McIntyre CK. Rapid remission of conditioned fear expression with extinction training paired with vagus nerve stimulation. Biol Psychiatry 2013;73(11):1071-7.
7. Sjögren MJ, Hellström PT, Jonsson MA, Runnerstam M, Silander HC, Ben-Menachem E. Cognition-enhancing effect of vagus nerve stimulation in patients with Alzheimer's disease: a pilot study. J Clin Psychiatry 2002;63(11):972-80.
8. Bodenlos JS, Kose S, Borckardt JJ, Nahas Z, Shaw D, O'Neil PM, et al. Vagus nerve stimulation acutely alters food craving in adults with depression. Appetite 2007;48(2):145-53.
9. Henry TR. Therapeutic mechanisms of vagus nerve stimulation. Neurology 2002;59(6 suppl 4):S3-S14.
10. Beaumont E, Campbell RBP, Andresen MC, Scofield SL, Singh K, Libbus I, et al. Clinically-styled vagus nerve stimulation augments spontaneous discharge in second and higher order sensory neurons in rat nucleus of the solitary tract. American Journal of Physiology-Heart and Circulatory Physiology 2017:ajpheart. 00070.2017.
11. Groves DA, Bowman EM, Brown VJ. Recordings from the rat locus coeruleus during acute vagal nerve stimulation in the anaesthetised rat. Neuroscience letters 2005;379(3):174-9.
12. Larsen LE, Wadman WJ, Marinazzo D, van Mierlo P, Delbeke J, Daelemans S, et al. Vagus nerve stimulation applied with a rapid cycle has more profound influence on hippocampal electrophysiology than a standard cycle. Neurotherapeutics 2016;13(3):592-602.
13. Chase MH, Nakamura Y, Clemente CD, Sterman MB. Afferent vagal stimulation: neurographic correlates of induced EEG synchronization and desynchronization. Brain Res 1967;5(2):236-49.
14. Bartolomei F, Bonini F, Vidal E, Trébuchon A, Lagarde S, Lambert I, et al. How does vagal nerve stimulation (VNS) change EEG brain functional connectivity? Epilepsy Res 2016;126:141-6.
15. Ressler KJ, Mayberg HS. Targeting abnormal neural circuits in mood and anxiety disorders: from the laboratory to the clinic. Nature neuroscience 2007;10(9):1116.
16. Garnett ES, Nahmias C, Scheffel A, Firnau G, Upton AR. Regional cerebral blood flow in man manipulated by direct vagal stimulation. Pacing Clin Electrophysiol 1992;15(10 Pt 2):1579-80.
17. Ko D, Heck C, Grafton S, Apuzzo ML, Couldwell WT, Chen T, et al. Vagus nerve stimulation activates central nervous system structures in epileptic patients during PET H2(15)O blood flow imaging. Neurosurgery 1996;39(2):426-30; discussion 30-1.
18. Henry TR, Votaw JR, Pennell PB, Epstein CM, Bakay RA, Faber TL, et al. Acute blood flow changes and efficacy of vagus nerve stimulation in partial epilepsy. Neurology 1999;52(6):1166-73.

433 19. Zobel A, Joe A, Freymann N, Clusmann H, Schramm J, Reinhardt M, et al. Changes in regional
434 cerebral blood flow by therapeutic vagus nerve stimulation in depression: an exploratory approach.
435 Psychiatry Res 2005;139(3):165-79.
436 20. Devous M, Husain M, Harris T, Rush A. Effects of VNS on regional cerebral blood flow in
437 depressed subjects. European Psychiatry 2002;17:113-4.
438 21. Sucholeiki R, Alsaadi TM, Morris Iii GL, Ulmer JL, Biswal B, Mueller WM. fMRI in patients
439 implanted with a vagal nerve stimulator. Seizure 2002;11(3):157-62.
440 22. Liu W-C, Mosier K, Kalnin A, Marks D. Vagus Nerve Stimulation in patients: a BOLD fMRI study.
441 NeuroImage 2001;13(6):810.
442 23. Bohning DE, Lomarev MP, Denslow S, Nahas Z, Shastri A, George MS. Feasibility of vagus nerve
443 stimulation–synchronized blood oxygenation level–dependent functional MRI. Investigative Radiology
444 2001;36(8):470-9.
445 24. Lomarev M, Denslow S, Nahas Z, Chae JH, George MS, Bohning DE. Vagus nerve stimulation
446 (VNS) synchronized BOLD fMRI suggests that VNS in depressed adults has frequency/dose dependent
447 effects. J Psychiatr Res 2002;36(4):219-27.
448 25. Chae JH, Nahas Z, Lomarev M, Denslow S, Lorberbaum JP, Bohning DE, et al. A review of
449 functional neuroimaging studies of vagus nerve stimulation (VNS). J Psychiatr Res 2003;37(6):443-55.
450 26. Krahl SE, Clark KB, Smith DC, Browning RA. Locus coeruleus lesions suppress the seizure-
451 attenuating effects of vagus nerve stimulation. Epilepsia 1998;39(7):709-14.
452 27. Nichols JA, Nichols AR, Smirnakis SM, Engineer ND, Kilgard MP, Atzori M. Vagus nerve
453 stimulation modulates cortical synchrony and excitability through the activation of muscarinic receptors.
454 Neuroscience 2011;189:207-14.
455 28. Fang J, Rong P, Hong Y, Fan Y, Liu J, Wang H, et al. Transcutaneous vagus nerve stimulation
456 modulates default mode network in major depressive disorder. Biological psychiatry 2016;79(4):266-73.
457 29. Biswal B, Zerrin Yetkin F, Haughton VM, Hyde JS. Functional connectivity in the motor cortex of
458 resting human brain using echo-planar mri. Magnetic resonance in medicine 1995;34(4):537-41.
459 30. Van Den Heuvel MP, Pol HEH. Exploring the brain network: a review on resting-state fMRI
460 functional connectivity. European neuropsychopharmacology 2010;20(8):519-34.
461 31. Pawela CP, Biswal BB, Hudetz AG, Schulte ML, Li R, Jones SR, et al. A protocol for use of
462 medetomidine anesthesia in rats for extended studies using task-induced BOLD contrast and resting-
463 state functional connectivity. Neuroimage 2009;46(4):1137-47.
464 32. Glover GH, Li TQ, Ress D. Image-based method for retrospective correction of physiological
465 motion effects in fMRI: RETROICOR. Magn Reson Med 2000;44(1):162-7.
466 33. Birn RM, Diamond JB, Smith MA, Bandettini PA. Separating respiratory-variation-related
467 fluctuations from neuronal-activity-related fluctuations in fMRI. Neuroimage 2006;31(4):1536-48.
468 34. Valdés-Hernández PA, Sumiyoshi A, Nonaka H, Haga R, Aubert-Vásquez E, Ogawa T, et al. An in
469 vivo MRI template set for morphometry, tissue segmentation, and fMRI localization in rats. Frontiers in
470 neuroinformatics 2011;5.
471 35. Nahas Z, Teneback C, Jeong-Ho C, Mu Q, Molnar C, Kozel FA, et al. Serial vagus nerve stimulation
472 functional MRI in treatment-resistant depression. Neuropsychopharmacology 2007;32(8):1649.
473 36. Kraus T, Kiess O, Hösl K, Terekhin P, Kornhuber J, Forster C. CNS BOLD fMRI effects of sham-
474 controlled transcutaneous electrical nerve stimulation in the left outer auditory canal–a pilot study.
475 Brain stimulation 2013;6(5):798-804.
476 37. Kraus T, Hösl K, Kiess O, Schanze A, Kornhuber J, Forster C. BOLD fMRI deactivation of limbic and
477 temporal brain structures and mood enhancing effect by transcutaneous vagus nerve stimulation. J
478 Neural Transm. 2007;114(11):1485-93.
479 38. Bell AJ, Sejnowski TJ. An information-maximization approach to blind separation and blind
480 deconvolution. Neural computation 1995;7(6):1129-59.

39. Beckmann CF, Smith SM. Probabilistic independent component analysis for functional magnetic resonance imaging. IEEE transactions on medical imaging 2004;23(2):137-52.
40. Ma Z, Perez P, Liu Y, Hamilton C, Liang Z, Zhang N. Functional atlas of the awake rat brain: A neuroimaging study of rat brain specialization and integration. Neuroimage 2016.
41. Schölvinck ML, Maier A, Frank QY, Duyn JH, Leopold DA. Neural basis of global resting-state fMRI activity. Proceedings of the National Academy of Sciences 2010;107(22):10238-43.
42. Gonzalez-Castillo J, Saad ZS, Handwerker DA, Inati SJ, Brenowitz N, Bandettini PA. Whole-brain, time-locked activation with simple tasks revealed using massive averaging and model-free analysis. Proc Natl Acad Sci U S A 2012;109(14):5487-92.
43. Lee JH, Durand R, Gradinaru V, Zhang F, Goshen I, Kim D-S, et al. Global and local fMRI signals driven by neurons defined optogenetically by type and wiring. Nature 2010;465(7299):788.
44. Paxinos G. The rat nervous system: Academic press; 2014.
45. Van Bockstaele EJ, Peoples J, Valentino RJ. A.E. Bennett Research Award. Anatomic basis for differential regulation of the rostrolateral peri-locus coeruleus region by limbic afferents. Biol Psychiatry 1999;46(10):1352-63.
46. Dorr AE, Debonnel G. Effect of vagus nerve stimulation on serotonergic and noradrenergic transmission. J Pharmacol Exp Ther 2006;318(2):890-8.
47. Manta S, Dong J, Debonnel G, Blier P. Enhancement of the function of rat serotonin and norepinephrine neurons by sustained vagus nerve stimulation. J Psychiatry Neurosci 2009;34(4):272-80.
48. Ruffoli R, Giorgi FS, Pizzanelli C, Murri L, Paparelli A, Fornai F. The chemical neuroanatomy of vagus nerve stimulation. J Chem Neuroanat 2011;42(4):288-96.
49. Frangos E, Komisaruk BR. Access to vagal projections via cutaneous electrical stimulation of the neck: fMRI evidence in healthy humans. Brain stimulation 2017;10(1):19-27.
50. Renvall V, Hari R. Transients may occur in functional magnetic resonance imaging without physiological basis. Proc Natl Acad Sci U S A 2009;106(48):20510-4.
51. Tyler CW, Kontsevich LL, Ferree TC. Independent components in stimulus-related BOLD signals and estimation of the underlying neural responses. Brain Res 2008;1229:72-89.
52. Obata T, Liu TT, Miller KL, Luh WM, Wong EC, Frank LR, et al. Discrepancies between BOLD and flow dynamics in primary and supplementary motor areas: application of the balloon model to the interpretation of BOLD transients. Neuroimage 2004;21(1):144-53.
53. Ma Y, Shaik MA, Kozberg MG, Kim SH, Portes JP, Timerman D, et al. Resting-state hemodynamics are spatiotemporally coupled to synchronized and symmetric neural activity in excitatory neurons. Proc Natl Acad Sci U S A 2016;113(52):E8463-E71.
54. Zabara J. Inhibition of experimental seizures in canines by repetitive vagal stimulation. Epilepsia 1992;33(6):1005-12.
55. Anastassiou CA, Shai AS. Psyche, Signals and Systems. Micro-, Meso-and Macro-Dynamics of the Brain: Springer; 2016. p. 107-56.
56. Tian P, Teng IC, May LD, Kurz R, Lu K, Scadeng M, et al. Cortical depth-specific microvascular dilation underlies laminar differences in blood oxygenation level-dependent functional MRI signal. Proceedings of the National Academy of Sciences 2010;107(34):15246-51.
57. Bush G, Luu P, Posner MI. Cognitive and emotional influences in anterior cingulate cortex. Trends in cognitive sciences 2000;4(6):215-22.
58. Vogt BA, Finch DM, Olson CR. Functional heterogeneity in cingulate cortex: the anterior executive and posterior evaluative regions. Cerebral cortex 1992;2(6):435-43.
59. Balleine BW, Delgado MR, Hikosaka O. The role of the dorsal striatum in reward and decision-making. Journal of Neuroscience 2007;27(31):8161-5.

527 60. Parkinson JA, Willoughby PJ, Robbins TW, Everitt BJ. Disconnection of the anterior cingulate
528 cortex and nucleus accumbens core impairs Pavlovian approach behavior: Further evidence for limbic
529 cortical–ventral striatopallidal systems. Behavioral neuroscience 2000;114(1):42.
530 61. Sackeim HA, Rush AJ, George MS, Marangell LB, Husain MM, Nahas Z, et al. Vagus nerve
531 stimulation (VNS (TM)) for treatment-resistant depression: efficacy, side effects, and predictors of
532 outcome. Neuropsychopharmacology 2001;25(5):713.
533 62. Nemeroff CB, Mayberg HS, Krahl SE, McNamara J, Frazer A, Henry TR, et al. VNS therapy in
534 treatment-resistant depression: clinical evidence and putative neurobiological mechanisms.
535 Neuropsychopharmacology 2006;31(7):1345.
536 63. Schwarz LA, Luo L. Organization of the locus coeruleus-norepinephrine system. Current Biology
537 2015;25(21):R1051-R6.
538 64. Mesulam M, Mufson E, Wainer B, Levey A. Central cholinergic pathways in the rat: an overview
539 based on an alternative nomenclature (Ch1–Ch6). Neuroscience 1983;10(4):1185-201.
540 65. Friston KJ, Fletcher P, Josephs O, Holmes A, Rugg M, Turner R. Event-related fMRI: characterizing
541 differential responses. Neuroimage 1998;7(1):30-40.
542 66. Li B, Freeman RD. Neurometabolic coupling in the lateral geniculate nucleus changes with
543 extended age. Journal of neurophysiology 2010;104(1):414-25.
544 67. Kundu P, Brenowitz ND, Voon V, Worbe Y, Vértes PE, Inati SJ, et al. Integrated strategy for
545 improving functional connectivity mapping using multiecho fMRI. Proceedings of the National Academy
546 of Sciences 2013;110(40):16187-92.
547 68. Zaaimi B, Grebe R, Wallois F. Animal model of the short-term cardiorespiratory effects of
548 intermittent vagus nerve stimulation. Auton Neurosci 2008;143(1-2):20-6.
549 69. Murray BJ, Matheson JK, Scammell TE. Effects of vagus nerve stimulation on respiration during
550 sleep. Neurology 2001;57(8):1523-4.
551 70. Reyt S, Picq C, Sinniger V, Clarençon D, Bonaz B, David O. Dynamic Causal Modelling and
552 physiological confounds: a functional MRI study of vagus nerve stimulation. Neuroimage 2010;
553 52(4):1456-64.
554 71. Sierakowiak A, Monnot C, Aski SN, Uppman M, Li T-Q, Damberg P, et al. Default mode network,
555 motor network, dorsal and ventral basal ganglia networks in the rat brain: comparison to human
556 networks using resting state-fMRI. PloS one 2015;10(3):e0120345.
557 72. Viswanathan A, Freeman RD. Neurometabolic coupling in cerebral cortex reflects synaptic more
558 than spiking activity. Nature neuroscience 2007;10(10):1308.

559

560

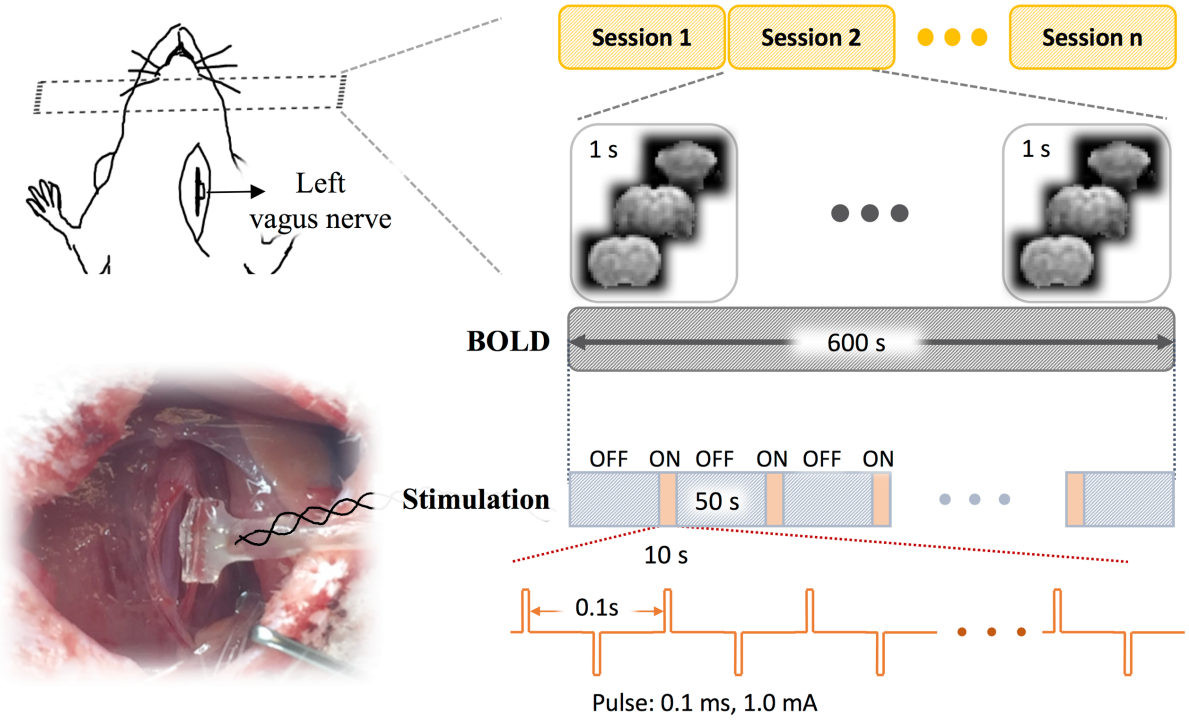

Figure 1. Experimental design. Each rat was electrically stimulated at the left cervical vagus through a cuff electrode implanted in an acute surgery. The stimulation (0.1ms pulse width, 1.0mA amplitude, 10Hz) was delivered in a 10s-ON-50s-OFF cycle, while the rat was scanned for fMRI with 1s TR.

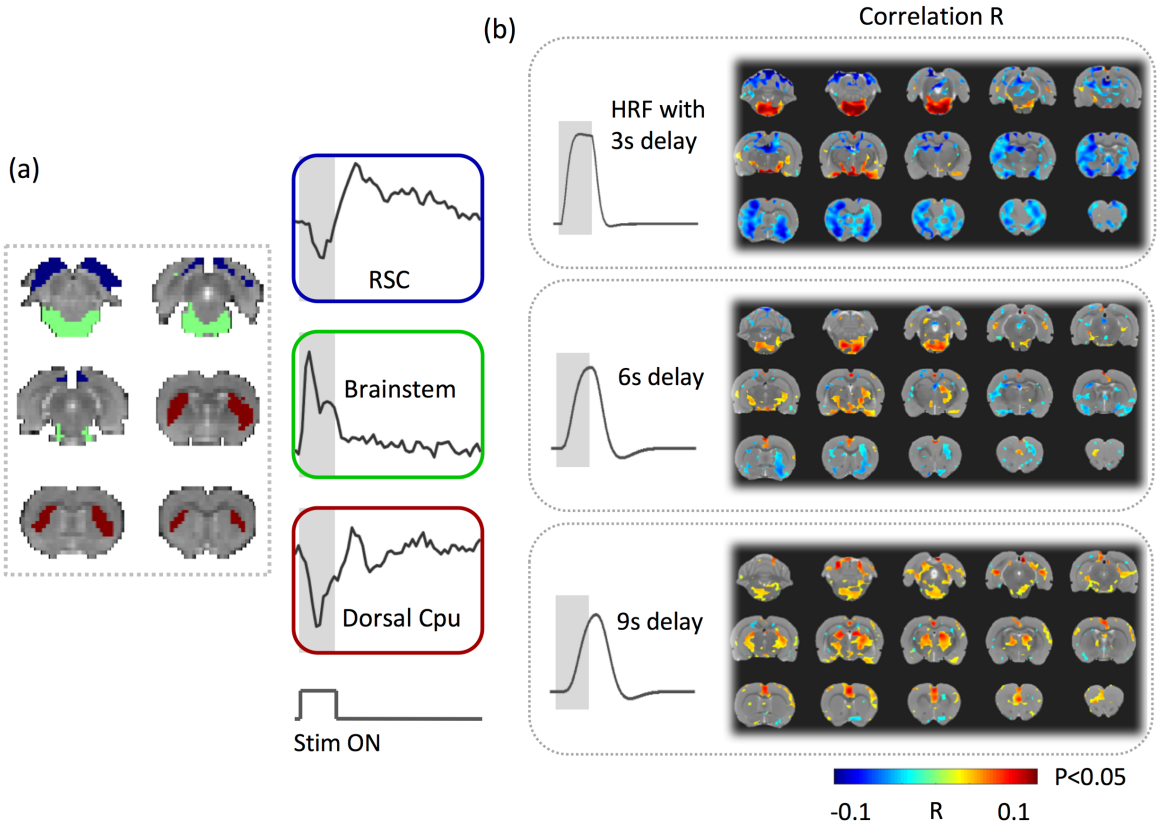

Figure 2. VNS-evoked responses varied across regions. (a) shows the response time series averaged within each of the three color-coded regions of interest shown: the retrosplenial cortex (RSC) (blue), the brainstem, and the dorsal caudate putamen (Cpu). (b) shows the highly different activation maps based on the response models derived with the HRF, for which different peak latencies were assumed to be 3s, 6s, or 9s.

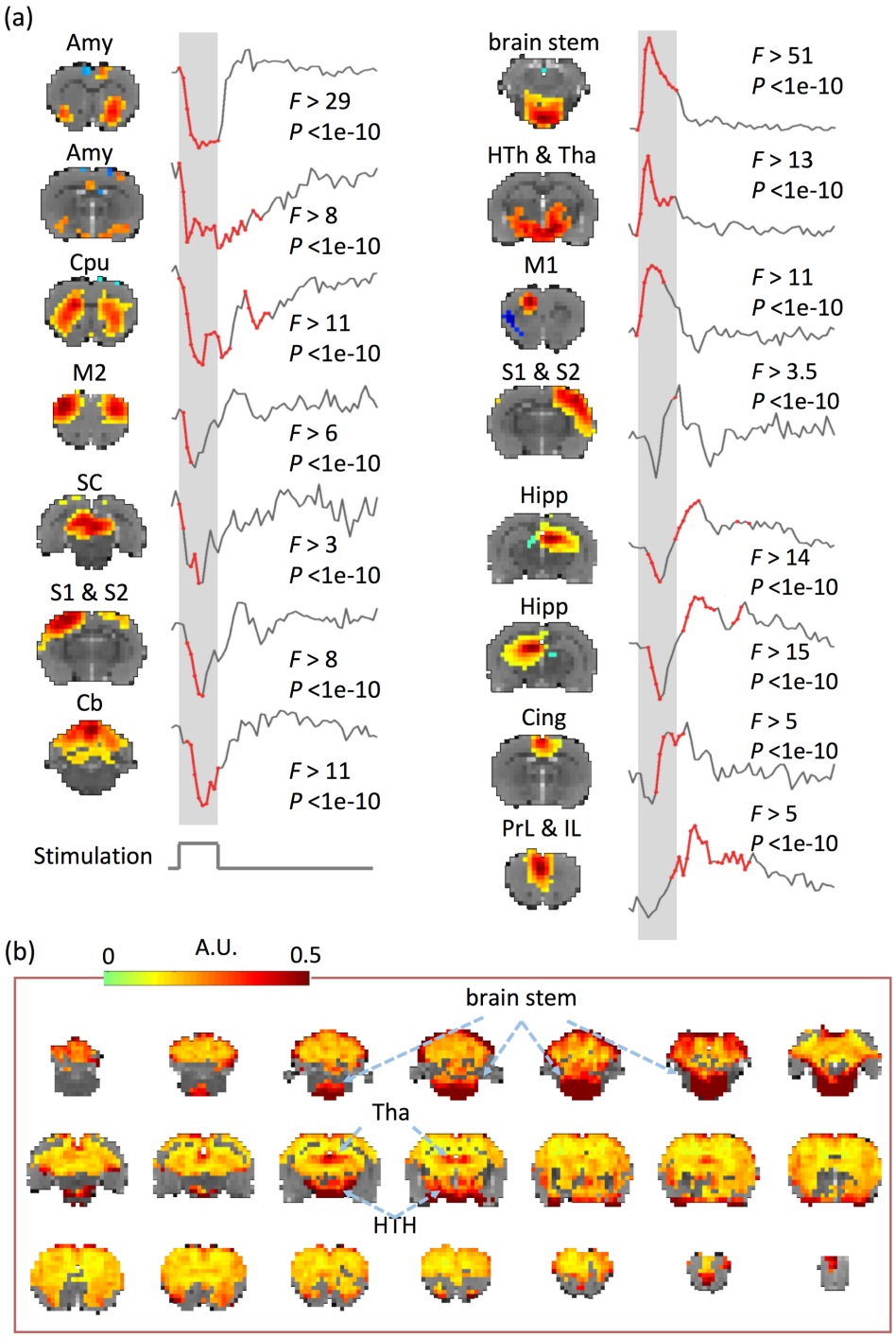

571

572 **Figure 3**. VNS evoked widespread and complex responses in the brain. (**a**) VNS-evoked responses for

573 different brain networks derived with ICA. The ICA-defined networks are labeled: amygdala (Amy),

574 caudate putamen (Cpu), hippocampus, (Hipp), cingulate cortex (Cing), prelimbic cortex (PrL), infralimbic
575 cortex (IL), brain stem, hypothalamus (HTh), thalamus (Tha), superior colliculus (SC), cerebellum (Cb),
576 primary and secondary motor cortex (M1, M2), and primary and secondary somatosensory cortex (S1,
577 S2). For each network, the time points at which the responses were significant are shown in red. (**b**) The
578 VNS-activated voxels cover 76.03% of the brain volume. The color is in arbitrary units, representing the
579 standard deviation of the voxel-wise response averaged across repetitions of VNS. The locations with the
580 greatest responses are highlighted with arrows.

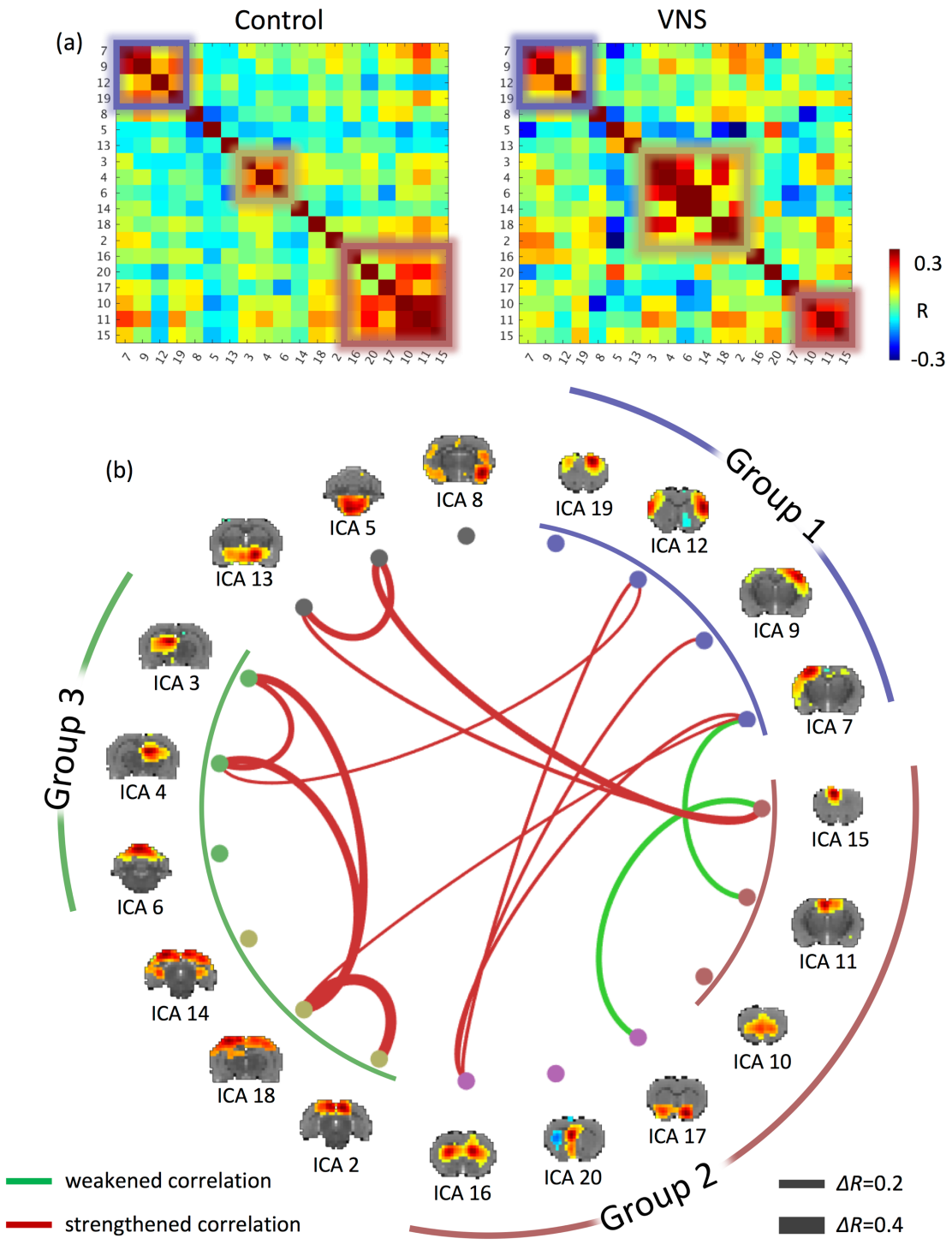

581

582 **Figure 4**. VNS altered the functional connectivity among intrinsic functional networks. (**a**) shows the

583 network-network correlations between independent components derived with ICA. The left shows the

correlation matrix during the resting state, or the "control" condition. The right shows the correlation matrix during VNS, or the "VNS" condition. Smaller squares highlight the networks (or ICs) that were clustered into groups (based on k-means clustering). (**b**) shows the IC-IC functional connectivity that was significantly different between the VNS and control conditions (t-test, $P<0.005$). Red lines represent increases in functional connectivity, and green lines represent decreases in functional. The thickness of the lines represents the (VNS versus control) change in correlation. The brain maps show the spatial patterns of individual ICs. Corresponding to the squares in (a), the arc lines illustrate how the ICs were clusters into groups, for the VNS condition (inner circle) and the control condition (outer circle).